0.5 h, (+)-(*R*)-(η^5-C_5H_5)Re(NO)(PPh_3)(Br) precipitated as a purple powder. The combined hexane extracts were passed through a pipette containing a small plug of silica gel. Solvent was removed by blowing a stream of nitrogen into the receiving vial, leaving a clear colorless oil. Then nonlabeled carrier dimethoxytoluene (31.3 mg, 0.206 mmol) was added, and the mixture was purified by column chromatography (silica gel 60, 230–400 mesh, Merck; 10 g) using 1:1 (v/v) hexanes/$CHCl_3$. Solvent was removed under a nitrogen stream to give (*R*)-**5** as a colorless oil (332 μCi, 87% radiochemical yield, 85% chemical yield).

Preparation of (*S*)-3,5-Dimethoxytoluene-α-d_1t_1 ((*S*)-5). A 10-mL pear-shaped flask was charged with (−)-(*RR*)-**3**-α-d_1t_1 (0.035 g, 0.050 mmol, 1.29 mCi), and CH_2Cl_2 (2 mL). The homogeneous solution was freeze–thaw–degassed (3×) and placed in a bath at −78 °C. Then 48% aqueous HBr (7 μL, 0.65 mmol) was added and the solution stirred for 12 h while gradually warming to room temperature. The solvent was removed by blowing a stream of nitrogen into the flask leaving a maroon oil. Hexanes were added to the flask, and after the mixture was stirred for 0.5 h, (−)-(*S*)-(η^5-C_5H_5)Re(NO)(PPh_3)(Br) precipitated as a purple powder. The combined hexane extracts were passed through a pipette containing a small plug of silica gel. Solvent was removed under nitrogen stream to give (*S*)-**5** as a colorless oil (7.20 mg, 0.0471 mmol, 94% chemical yield).

Preparation of (*S*)-CHDTCOO$^-$Na$^+$ and (*R*)-CHDTCOO$^-$Na$^+$. Nonlabled carrier 3,5-dimethoxytoluene (45 mg, 0.30 mmol) was added to a sample of (*S*)-**5**, and the mixture was passed through a silica gel column (silica gel 60, 230–400 mesh, Merck; 10 g) using hexane/$CHCl_3$ (1:1 v/v). To a solution of the resulting (*S*)-**5** (0.2 mmol, 1.0×10^8 dpm, 48 μCi) in *n*-hexane (5 mL) was added silicic acid (3 g, 100 mesh, Mallinckrodt), and the solvent was removed in vacuo. The resulting silicic acid with absorbed substrate was stirred for 2 h at −78 °C under a stream of ozone. The sample was kept at room temperature for 1 h, and the ozonolysis was repeated (2 h, −78 °C). The mixture was warmed to 4 °C, and water (10 mL) was added. The suspension was kept at 4 °C overnight and then steam distilled. The distillate (120 mL) was neutralized with 0.1 N NaOH and evaporated to dryness. The residue was dissolved in water (90 mL), mixed with $HgSO_4$ (0.9 g) and concentrated H_2SO_4 (1.5 mL), and steam distilled. Neutralization of the distillate and evaporation to dryness as above gave (*S*)-CHDTCOO$^-$Na$^+$ (5.2×10^7 dpm) in 50% radiochemical yield. The *F* value of this material was found to be 23.[7] Similarly, (*R*)-**5** (0.2 mmol, 0.051 μCi) gave (*R*)-CHDTCOO$^-$Na$^+$ (9.6×10^3 dpm) with $F = 75$.

Acknowledgment. We thank the NIH for support of this research (Utah, GM 31280-05; Ohio State, GM 32333-04) and the C. D. Poulter group for helpful discussions and use of their radiochemical laboratory. The NMR spectrometers utilized were acquired via NSF, DOD, and NIH instrumentation grants.

Cation Distributions within a Cluster Framework. Synthesis and Structure of the Carbon- and Boron-Centered Zirconium Cluster Compounds $KZr_6Cl_{15}C$ and $CsKZr_6Cl_{15}B$

Robin P. Ziebarth and John D. Corbett*

Contribution from the Department of Chemistry, Iowa State University, Ames, Iowa 50011.
Received December 24, 1986

Abstract: The structures of the isotypic $KZr_6Cl_{15}C$ and $CsKZr_6Cl_{15}B$ have been established by single-crystal X-ray diffraction in space group *Pmma*, $Z = 4$ ($R = 3.1$, 3.9%; $R_w = 3.2$, 3.6%, respectively). These contain a matrix of Z-centered $Zr_6Cl_{12}Z$ clusters linked together by trans-chlorine atoms to form separate linear and zigzag chains that are interconnected into a three-dimensional network by four additional bridging chlorides. This $(Zr_6Cl_{12}Z)Cl_{6/2}$ framework affords three types of chloride environments for the cations, a smaller one (a) of ten-coordination occupied by potassium or rubidium and a pair of larger sites (b) with lower multiplicity that are utilized by cesium etc. The two b-type metal sites exhibit (1) an elongated square-pyramidal environment which, for the matrix studied, leaves the cesium closer to four-coordinate and (2) a more distorted 6 + 2 position of $2/m$ symmetry. Some evident cation disorder especially in the b(2) site and a possible small distortion of the anion matrix are noted. Compounds of this type are made by the reaction of stoichiometric amounts of $ZrCl_4$ and Zr with C, B, or ZrNCl and the appropriate MCl in welded Ta containers at 850 °C. These reactions give, according to Guinier powder diffraction, >95% yields of $KZr_6Cl_{15}Z$, Z = C or N, with occupancy of cation site a, the isotopic (Cs or Rb)$Zr_6Cl_{15}C$ utilizing site b, and (CsK, Rb_2, or CsRb)$Zr_6Cl_{15}B$ with a and b site occupancy. All but the nitride involve 14 cluster-bonding electrons, the most preferred state according to the MO scheme. The cluster framework and the cation bonding in this structure are compared with those in four other structure types that are known for $M_6X_{12}X_{6/2}$-type compounds.

Over the past several years, an increasing number of octahedral metal clusters that require a heteroatom within the cluster for stability have been reported within rare-earth-metal and early-transition-metal halides.[1-6] As a result of these investigations, it is becoming increasingly evident that many, but not all, of the previously prepared clusters and condensed clusters of these elements that were implicitly presumed to be empty actually are interstitially stabilized by small nonmetals. Prime examples are Zr_6Cl_{15}, Sc_5Cl_8, and the rare-earth-metal monohalides which are now recognized to be the halide mononitride, carbide, and hydrides, respectively.[1,7-9]

These results also suggest that a vast and largely untapped potential exists for the preparation of new cluster compounds by the purposeful and systematic addition of potential interstitial elements to cluster-forming reactions. The potential lies not only

(1) Ziebarth, R. P.; Corbett, J. D. *J. Am. Chem. Soc.* **1985**, *107*, 4571.
(2) Smith, J. D.; Corbett, J. D. *J. Am. Chem. Soc.* **1985**, *107*, 5704.
(3) Smith, J. D.; Corbett, J. D. *J. Am. Chem. Soc.* **1986**, *108*, 1927.
(4) Hwu, S.-J.; Corbett, J. D. *J. Solid State Chem.* **1986**, *64*, 331.
(5) Dudis, D. S.; Corbett, J. D. *Inorg. Chem.* **1986**, *25*, 3434.
(6) Hughbanks, T. R.; Rosenthal, G.; Corbett, J. D. *J. Am. Chem. Soc.* **1986**, *108*, 8289.
(7) Hwu, S.-J.; Dudis, D. S.; Corbett, J. D. *Inorg. Chem.* **1987**, *26*, 469.
(8) Simon, A. *J. Solid State Chem.* **1985**, *57*, 2.
(9) Meyer, G.; Hwu, S.-J.; Wijeyesekera, S.; Corbett, J. D. *Inorg. Chem.* **1986**, *25*, 4811.

0002-7863/87/1509-4844$01.50/0

Table I. Lattice Parameters (Å) and Cell Volumes (Å^3) for the $Zr_6Cl_{15}Z$-Type Compounds Studied[a]

compd	*a*	*b*	*c*	*V*	cation site type[b]
$KZr_6Cl_{15}C$	18.489 (5)	13.909 (3)	9.690 (3)	2492 (1)	a
$RbZr_6Cl_{15}C$	18.468 (5)	13.891 (4)	9.648 (3)	2475 (1)	b
$CsZr_6Cl_{15}C$	18.509 (4)	13.923 (3)	9.646 (2)	2485.6 (9)	b
$CsKZr_6Cl_{15}B$	18.672 (4)	14.026 (4)	9.731 (2)	2548 (1)	a + b
$Rb_2Zr_6Cl_{15}B$	18.666 (2)	14.033 (2)	9.757 (1)	2555.8 (6)	a + b
$CsRbZr_6Cl_{15}B$	18.703 (2)	14.087 (2)	9.771 (1)	2574.4 (5)	a + b
$KZr_6Cl_{15}N$	18.292 (2)	13.824 (1)	9.590 (1)	2425.1 (5)	a
$CsZr_6Br_{15}Fe$[c]	19.721 (3)	14.863 (3)	10.265 (2)	3009 (1)	b

[a] Guinier powder diffraction data. [b] See text. [c] Reference 10.

in the ability to alter the number of cluster electrons and hence the electronic properties of a cluster by changing the interstitial element but also in an ability to generate completely new structural arrangements of clusters and novel stoichiometries. The potential of the latter has now been at least partially realized with the zirconium chlorides where eight new structures types and two new stoichiometries for M_6X_{12}-types cluster phases have been obtained together with many variations that also contain alkali-metal cations.[1,10]

Herein we report in detail the syntheses and structures of $KZr_6Cl_{15}C$ and $CsKZr_6Cl_{15}B$ as well as the preparation of the related compounds $RbZr_6Cl_{15}C$, $CsZr_6Cl_{15}C$, $KZr_6Cl_{15}N$, $Rb_2Zr_6Cl_{15}B$, and $CsRbZr_6Cl_{15}B$. All of their structures are based on a common $(Zr_6Cl_{12})Cl_{6/2}$ framework, where the Zr_6Cl_{12} core consists of a nominal octahedron of zirconium that has all edges bridged by (inner) chlorine atoms. However, the availability and occupation of more than one set of cation sites within this matrix generates some interesting variations as well as complications. A brief description of the bonding within these clusters is also provided.

Experimental Section

Materials. Reactor-grade crystal bar zirconium (<500 ppm Hf) was used to prepare Zr powder via the thermal decomposition of ZrH_{2-x} in high vacuum, as previously described.[2] The $ZrCl_4$ employed was prepared by the direct reaction of the elements at 300–350 °C and was purified by three successive vaccum sublimations over Zr metal and through a coarse-grade Pyrex frit. Reagent-grade alkali-metal chlorides were slowly dried and then purified by vacuum sublimation. Spectroscopic grade graphite (National Brand, Union Carbide) and amorphous boron powder (95%, 325 mesh, Alfa) were degassed under dynamic vacuum at 850 °C prior to use. ZrNCl was prepared by passing NH_3 over $ZrCl_4$ at 600 °C.

Syntheses. Because of the air- and moisture-sensitive nature of many of the reactants and products, all materials were handled under vacuum or inert-atmosphere conditions. The preparations typically utilized stoichiometric quantities of Zr powder and $ZrCl_4$ together with graphite, boron, or ZrNCl and the appropriate M^ICl. A small excess of $ZrCl_4$ was added to each reaction to allow for the autogeneous $ZrCl_4$ pressure (~2–4 atm) over the cluster product at temperature. The reactions were carried out in welded Ta tubing encased in evacuated and sealed jackets of fused silica. The systems were usually heated to 850 °C over a 24-h period, equilibrated for 2 weeks, and then air quenched. The product distributions in these reactions are largely controlled by the initial ratio of the reactants. For example, $RbZr_6Cl_{14}B$, $Rb_2Zr_6Cl_{15}B$, and $Rb_5Zr_6Cl_{18}B$[10] can all be prepared from $Zr/ZrCl_4/B$ mixtures simply by varying the amount of RbCl present.

The products obtained under the appropriate conditions were single phase as judged by careful examination of Guinier powder diffraction patterns and by microscopic inspection of the reaction products. The former means that powder data were consistent not only in position but also in intensity with those in the pattern calculated by using the indicated lattice constants and positional parameters for the known structure type. The high yields, estimated to be in excess of 95% when the correct stoichiometric proportions are used, are an important factor in establishing the identity of the interstitial element since X-ray diffraction cannot be counted on to distinguish reliably among light non-metal atoms such as B, C, or N. All of the $M^I_xZr_6Cl_{15}$ carbides ($x = 1$) and borides ($x = 2$) occur as black microcrystalline powders mixed with some larger well-faceted, very dark red parallelepipeds. Several of the compounds have also been observed as very thin, dark red rods or blades, apparently formed by slow chemical transport when reactions were run under a 20–30 °C temperature gradient. Recognizable single crystals were not obtained for the nitride.

Table II. Summary of Crystal and Diffraction Data for $KZr_6Cl_{15}C$ and $CsKZr_6Cl_{15}B$

	$KZr_6Cl_{15}C$	$CsKZr_6Cl_{15}B$
space group[a]	*Pmma* (No. 51)	*Pmma*
Z	4	4
a, Å	18.489 (5)	18.672 (4)
b, Å	13.909 (3)	14.026 (4)
c, Å	9.690 (3)	9.731 (2)
V, Å^3	2492 (1)	2548 (1)
cryst dimen, mm	0.35 × 0.25 × 0.15	0.45 × 0.20 × 0.15
scan mode; rate	ω-scan; fixed	ω-scan; variable
reflctns measured	h,k,l; $-h,-k,l$	$h,k,\pm l$; $h,-k,\pm l$
2θ(max), deg	55	55
μ(Mo Kα), cm^{-1}	40.9	54.4
transm coeff range[b]	0.70–1.00	0.83–1.00
measd refl	6613	12553
obs refl[c]	4725	7394
independent refl	2404	2144
R(av), %	4.3	3.3
secondary ext coeff	1.0 (2) × 10^{-4}	1.3 (3) × 10^{-5}
R,[d] %	3.1	3.9
R_w,[e] %	3.2	3.6

[a] See text. [b] Normalized. [c] $F_o \geq 3\sigma_F$ and $I_o > 3\sigma_I$. [d] $R = \sum||F_o| - |F_c||/\sum|F_o|$. [e] $R_w = [\sum w(|F_o| - |F_c|)^2/\sum w|F_o|^2]^{1/2}$; $w = 1/\sigma_F^2$ initially.

Powder Data. Lattice parameters used in distance calculations for both compounds were refined by least-squares fit of Guinier powder diffraction data of a sample obtained from the same reaction as the single crytal studied and with NBS Si powder as an internal standard. Lattice parameters for NBS α-Al_2O_3 obtained by this method deviate from the reference values by only 0.8 and 2.5 parts in 10^4. Lattice parameters for all of the compounds reported here are given in Table I.

Crystal Structure Determinations. Two octants of diffraction data were initially measured for both $KZr_6Cl_{15}C$ and $CsKZr_6Cl_{15}B$ at room temperature from nicely shaped, dark red rectangular prisms sealed under N_2 in 0.3-mm thin-walled glass capillaries. The measurements employed DATEX and SYNTEX diffractometers, respectively, Mo Kα radiation (λ = 0.710 69 Å), graphite monochromators, and 2θ limits of 55°. Data were later recollected for $CsKZr_6Cl_{15}B$ over four octants. Pertinent details of the data collections are contained in Table II.

For $KZr_6Cl_{15}C$, a primitive orthorhombic cell was chosen on the basis of 12 indexed reflections and was subsequently supported by the layer spacings and mirror symmetry seen in axial (Polaroid) photographs taken on the diffractometer. Axial photographs of $CsKZr_6Cl_{15}B$ taken on the diffractometer also confirmed the orthorhombic unit cell expected on the basis of Guinier powder diffraction patterns (below) and predicted by reflections indexed on the diffractometer. In addition, no evidence suggesting a higher or lower space group symmetry or a superlattice for the second compound was found on either oscillation or Weissenberg photographs.

No evidence of decay was noted during either data collection. Absorption effects, minimal because of the small absorption coefficients and nearly uniform crystal dimensions, were corrected empirically by using a ψ-scan method via intensity data from a single reflection tuned every 10° in φ. Programs used for absorption correction, data manipulation, and crystal structure refinement have been previously referenced.[11]

$KZr_6Cl_{15}C$. The space group *Pmma* (No. 51)[12] was established on the basis of the systematic extinctions apparently observed, an assumed

(10) Ziebarth, R. P.; Corbett, J. D., to be submitted for publication.

(11) Hwu, S.-J.; Corbett, J. D.; Poeppelmeier, K. R. *J. Solid State Chem.* **1985**, *57*, 43.

(12) *International Tables for Crystallography*; T. Hahn, Ed.; D. Reidel: Dordrecht, Holland, 1983; Vol. A, p 264. Some copies do not show all of the mirror planes clearly in the projections for *Pmma*.

Table III. Positional Parameters for $KZr_6Cl_{15}C$

	x	y	z
Zr(1)	0.47012 (2)	0.38378 (2)	0.34235 (3)
Zr(2)	0.61430 (2)	1/2	0.41815 (5)
Zr(3)	0.33785 (2)	0.11656 (2)	0.15743 (3)
Zr(4)	1/4	0	0.38799 (6)
Zr(5)	1/4	0	0.92519 (6)
Cl(1)	0.43822 (5)	0.25078 (7)	0.15795 (9)
Cl(2)	1/4	0	0.6571 (2)
Cl(3)	1/4	1/2	0.6837 (2)
Cl(4)	0	0.24508 (9)	1/2
Cl(5)	0.43405 (7)	1/2	0.1549 (1)
Cl(6)	0.59583 (5)	0.37143 (6)	0.23619 (9)
Cl(7)	0.33952 (4)	0.37381 (6)	0.41802 (9)
Cl(8)	1/4	0.25565 (9)	0.1505 (1)
Cl(9)	0.44244 (7)	0	0.1573 (1)
Cl(10)	0.34551 (5)	0.12701 (7)	0.41792 (8)
Cl(11)	0.15284 (5)	0.12775 (7)	0.89612 (9)
K	1/4	0.2529 (1)	0.6691 (2)
C(1)	1/2	1/2	1/2
C(2)	1/4	0	0.1562 (6)

centricity, and the successful refinement of the structure in this space group.

The structure was solved by the Patterson superposition method utilizing the program ALCAMPS[13] for map analysis. Twelve atom positions were identified and assigned to five zirconium and seven chlorine atoms, these being differentiated by interatomic distances and Patterson peak heights. The remaining atomic positions were identified by successive cycles of least-squares refinement and calculation of electron density maps. The potassium position was initially refined with a chlorine atom, but this was later replaced with the cation after it was observed that the atom had only chlorine nearest neighbors at distances of ~3.4 Å, about the sum of the K^+ and Cl^- radii. Refinement of the atomic positions and anisotropic thermal parameters of all atoms, except for carbon which was refined isotropically, proceeded smoothly and converged at $R = 0.031$ and $R_w = 0.032$, after reweighting. The weights were adjusted in a statistically meaningful way for 20–25 overlapping groups so as to minimize the dependence of $\sum w(|F_o| - |F_c|)^2$ on F_o. Refinement of the K, C(1), and C(2) occupancies did not result in values significantly different from unity (0.976 (8), 0.97 (3), and 1.06 (3), respectively), and these were hence fixed at full occupancy. A secondary extinction correction[11] was applied to the data after a comparison of $|F_o|$ vs. $|F_c|$ showed that the former was smaller for a disproportionate number of intense reflections. The final difference map was flat to less than ±0.25 e/Å^3.

$CsKZr_6Cl_{15}B$. The structure of $CsKZr_6Cl_{15}B$ was deduced by a comparison of its observed powder pattern with those calculated on the bases of the $CsNb_6Cl_{15}$[14] and $KZr_6Cl_{15}C$ structures, these differing only in the cation sites that are occupied. Least-squares refinement of the zirconium and chlorine positional parameters obtained for $KZr_6Cl_{15}C$ followed by a calculation of a Fourier map clearly showed the occupation of three additional sites in the lattice, corresponding to both the potassium position in $KZr_6Cl_{15}C$ (type a) and the two cesium positions in $CsNb_6Cl_{15}$ (b). Isotropic refinement proceeded smoothly to $R = 10.6\%$ with the inclusion of the indicated atoms. Boron atoms were included in the centers of the two independent clusters at this point and refined isotropically at unit occupancy while the rest of the atoms in the structure were refined anisotropically. Simultaneous refinement of occupancies of the three alkali metals, application of a secondary extinction correction, and a reweighting of the data set led to final values of $R = 0.039$ and $R_w = 0.036$. The potassium and cesium occupancies converged at somewhat more (1.27 (1)) and slightly less than unity (0.937 (6) and 0.784 (6)), respectively, indicating a small amount of cation mixing between sites (below). The final difference map was flat to less than ±0.5 e/Å^3. The largest peaks, 0.5 and 0.3 e/Å^3, were associated with Cs(1) and Cs(2), respectively.

The refined thermal ellipsoids for certain atoms in the $CsKZr_6Cl_{15}B$ structure indicated further consideration of the structure and its refinement was necessary, particularly with respect to supercells or lower space group symmetries. In contrast to the $KZr_6Cl_{15}C$ structure, which shows normal thermal parameters except for the somewhat flattened ellipsoids for the interconnected Zr(4)–Cl(2)$^{a-a}$–Cl(5) atoms along the linear cluster chain ($mm2$ symmetry), the $CsKZr_6Cl_{15}B$ refinement provides several examples of extreme thermal parameters. Most exceptional are

(13) Richardson, J. W., Jr.; Jacobson, R. A., Iowa State University, 1984, unpublished program.
(14) Imoto, H.; Simon, A., 1980, unpublished research.

Table IV. Positional Parameters for $CsKZr_6Cl_{15}B$

	x	y	z
Zr(1)	0.47097 (3)	0.38355 (4)	0.34042 (6)
Zr(2)	0.61493 (4)	1/2	0.4191 (1)
Zr(3)	0.33804 (3)	0.11672 (4)	0.14675 (6)
Zr(4)	1/4	0	0.3790 (1)
Zr(5)	1/4	0	0.9130 (1)
Cl(1)	0.4379 (1)	0.2509 (1)	0.1551 (2)
Cl(2)	1/4	0	0.6465 (4)
Cl(3)	1/4	1/2	0.6869 (4)
Cl(4)	0	0.2453 (1)	1/2
Cl(5)	0.4365 (1)	1/2	0.1503 (3)
Cl(6)	0.59714 (8)	0.3711 (1)	0.2378 (2)
Cl(7)	0.33966 (8)	0.3747 (1)	0.4130 (2)
Cl(8)	1/4	0.2556 (1)	0.1407 (3)
Cl(9)	0.4427 (1)	0	0.1501 (3)
Cl(10)	0.34515 (8)	0.1274 (1)	0.4093 (2)
Cl(11)	0.15269 (9)	0.1274 (1)	0.8856 (2)
K	1/4	0.2515 (1)	0.6588 (2)
Cs(1)	1/4	1/2	0.0911 (2)
Cs(2)	0	0	1/2
B(1)	1/2	1/2	1/2
B(2)	1/4	0	0.145 (1)

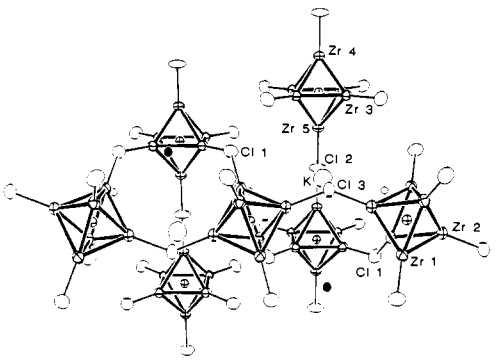

Figure 1. An approximately [010] view of the three-dimensional structure of $K[Zr_6(Cl^i)_{12}C](Cl^{a-a})_{6/2}$ with the c axis vertical. The zirconium atoms are connected by heavy lines while the Cl^i atoms have been omitted for clarity. One mirror plane parallel to the paper lies in the zigzag $Zr_6C(1)Cl(3)$ chain, and a second one normal to the figure contains the linear $Zr_6C(2)Cl(2)$ chain and K (90% probability thermal ellipsoids). The small solid and open circles mark the Cs(1) and Cs(2) (b type) positions, respectively, in $CsKZr_6Cl_{15}B$.

the two newly added cesium atoms. The inclusion of the cesium atoms in two rather unsymmetrical cavities in the cluster framework (see Structural Results) produces highly distorted thermal ellipsoids with principal axial ratios (and site symmetries) of 1.7:1:4.1 ($mm2$) and 1.3:1:16.1 ($2/m$) for Cs(1) and Cs(2), respectively (supplementary material). Attempts to refine Cs(2) in two inversion-related sites of equal occupancy failed to converge. Less remarkable disparities between principal axes of the ellipsoids also appear for other atoms that lie on symmetry elements in this space group, namely, Cl(3) ($mm2$), the bridging atom in the zigzag cluster chain Cl(4) (2), Cl(8) (m), and Cl(9) (m), with one axis or another being 33–44% of the largest. It is noteworthy that the latter group of chlorine atoms are all neighbors of one or the other of the cesium atoms that are new to the structure, and their thermal ellipsoids may therefore reflect more the character of the cation disposition than an intrinsic thermal property.

Considerable attention was given to the possibility that these "thermal" parameters actually reflected an error in the choice of space group or cell. The results of these considerations (supplementary material) leave us with the conclusion that particularly the cesium ellipsoids are reflections, in the harmonic description, of a real atom disorder in the crystal studied and not an error in space group symmetry. The thermal parameters in the potassium structure are much more well-behaved and, in fact, give a valuable base line from which we can better judge the $CsKZr_6Cl_{15}B$ results.

Structural Results

Final positional parameters for $KZr_6Cl_{15}C$ and $CsKZr_6Cl_{15}B$ are tabulated in Tables III and IV, respectively, and relevant interatomic distances are given in Table V. Thermal parameter and structure factor data are available as supplementary material.

Table V. Important Distances (Å) in $KZr_6Cl_{15}C$ (I) and $CsKZr_6Cl_{15}B$ (II)

	cluster 1 (zigzag chain)			cluster 2 (linear chain)	
	I	II		I	II
			Zr–Zr		
Zr(1)–Zr(2)	3.2028 (8)	3.2370 (9)	Zr(3)–Zr(4)	3.2028 (8)	3.239 (1)
Zr(1)–Zr(2)	3.2303 (8)	3.274 (1)	Zr(3)–Zr(5)	3.2141 (8)	3.249 (1)
Zr(1)–Zr(1)	3.2329 (9)	3.267 (1)	Zr(3)–Zr(3)	3.2424 (9)	3.274 (1)
Zr(1)–Zr(1)	3.249 (1)	3.290 (1)	Zr(3)–Zr(3)	3.248 (1)	3.288 (1)
$\bar{d}$	3.225	3.263		3.221	3.256
			$Zr–Cl^i$		
Zr(1)–Cl(4)	2.522 (1)	2.543 (2)	Zr(3)–Cl(8)	2.527 (1)	2.549 (2)
Zr(1)–Cl(5)	2.521 (1)	2.550 (2)	Zr(3)–Cl(9)	2.524 (1)	2.549 (2)
Zr(1)–Cl(6)	2.547 (1)	2.565 (2)	Zr(3)–Cl(10)	2.532 (1)	2.563 (2)
Zr(1)–Cl(7)	2.527 (1)	2.555 (2)	Zr(3)–Cl(11)	2.543 (1)	2.552 (2)
Zr(2)–Cl(6)	2.534 (1)	2.548 (2)	Zr(4)–Cl(10)	2.515 (1)	2.537 (2)
Zr(2)–Cl(7)	2.516 (1)	2.545 (2)	Zr(5)–Cl(11)	2.542 (1)	2.562 (2)
			$Zr–Cl^a$		
Zr(1)–Cl(1)	2.639 (1)	2.663 (2)	Zr(3)–Cl(1)	2.632 (1)	2.651 (2)
Zr(2)–Cl(3)	2.696 (1)	2.725 (2)	Zr(4)–Cl(2)	2.608 (2)	2.603 (4)
			Zr(5)–Cl(2)	2.598 (2)	2.593 (4)
			Zr–int		
Zr(1)–int(1)	2.2916 (5)	2.3179 (6)	Zr(3)–int(2)	2.2949 (5)	2.3201 (6)
Zr(2)–int(1)	2.2571 (7)	2.2860 (8)	Zr(4)–int(2)	2.247 (6)	2.27 (1)
			Zr(5)–int(2)	2.238 (6)	2.26 (1)
$\bar{d}$	2.2801	2.3073		2.277	2.302
			K–Cl		
K–Cl(2)	3.519 (2)	3.529 (2)			
K–Cl(3)	3.440 (2)	3.496 (2)			
K–Cl(6)	3.418 (2)	3.460 (2)			
K–Cl(7)	3.389 (2)	3.393 (2)			
K–Cl(10)	3.479 (2)	3.476 (2)			
K–Cl(11)	3.331 (2)	3.347 (2)			
$\bar{d}$	3.419	3.438			
			Cs–Cl		
Cs(1)–Cl(3)		3.933 (4)			
Cs(1)–Cl(5)		3.530 (2)			
Cs(1)–Cl(7)		3.963 (2)			
Cs(1)–Cl(8)		3.462 (2)			
Cs(2)–Cl(4)		3.440 (2)			
Cs(2)–Cl(9)		3.569 (3)			
Cs(2)–Cl(10)		3.511 (2)			

The structures of $KZr_6Cl_{15}C$ and $CsKZr_6Cl_{15}B$ are, like those of all other known M_6X_{15} compounds, composed of M_6X_{12}-type clusters with unshared, edge-bridging inner halogen X^i, and these are linked together through additional, shared terminal halogens $X^{a\text{-}a}$ at every metal vertex. The general arrangement is more succinctly described as $[M_6X^i_{12}]X^{a\text{-}a}{}_{6/2}$. The primary structural framework for these zirconium chlorides is identical with that of $CsNb_6Cl_{15}$[14] if the cations and interstitial atoms are neglected.

$KZr_6Cl_{15}C$. This structure can be viewed in terms of the two crystallographically independent chains of $Zr_6Cl_{12}C$ clusters that run in perpendicular directions and are interlinked by Cl(1) atoms. The illustration in Figure 1 of the two chains in $KZr_6Cl_{15}C$ will also serve as a description for $CsKZr_6Cl_{15}B$. One chain parallel to the *a* axis is split by the mirror plane at $y = {}^1/_2$ and exhibits bent $Cl^{a\text{-}a}$ linkages similar to those in Ta_6Cl_{15}.[15] It therefore has a zigzag appearance, with Zr–Cl(3)$^{a\text{-}a}$–Zr angles of ~140°. Each cluster in this chain has C_{2h} point symmetry and Zr–Zr distances that average 3.228 Å. The Zr–C distances in the compound average 2.28 Å which, when considered with the 0.86-Å crystal radius for ^{VI}Zr,[16] gives an effective carbon crystal radius of 1.42 Å. This value is slightly smaller than the 1.46-Å radius similarly derived from a number of rock-salt-type transition-metal monocarbides[2] but is the same as that from $Sc_7X_{12}C$ (X = Br, I)[5] and slightly larger than the 1.40-Å value for the more electron-rich $Zr_6I_{12}C$.[2]

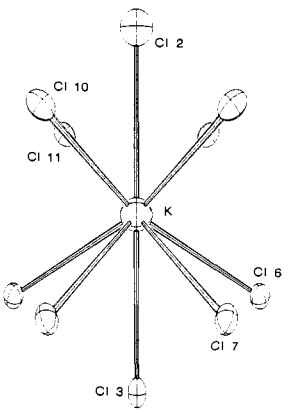

Figure 2. The potassium surroundings in $KZr_6Cl_{15}C$ (and $CsKZr_6Cl_{15}B$), with chain-bridging Cl(2) and Cl(3) at top and bottom, respectively. A vertical mirror plane lies normal to the drawing (50% ellipsoids).

A perpendicular chain runs parallel to the *c* axis and contains highly unusual Zr(4)–Cl(2)$^{a\text{-}a}$–Zr(5) linkages between clusters that are constrained to linearity by symmetry, the three atoms lying on the intersection of two mirror planes. This $Cl^{a\text{-}a}$ atom shows a platelike thermal ellipsoid perpendicular to the chain axis, consistent with either a greater thermal motion in what is presumably the most facile direction of vibration or some disordering around or small displacement of the chlorine atom from the axial site. The cluster in the linear chain shows a 0.05–0.06 Å compression along the pseudo-fourfold axis of the chain. The crys-

(15) Bauer, D.; von Schnering, H.-G. *Z. Anorg. Allg. Chem.* **1968**, *361*, 259.

(16) Shannon, R. D. *Acta Crystallogr., Sect. A: Cryst. Phys., Diffr., Theor., Gen. Crystallogr.* **1976**, *A32*, 751.

tallographically imposed symmetry is C_{2v}. The range and average of the Zr–Zr distances in this chain are very similar to those in the zigzag member, and the same is true of the Zr–C distances.

The four remaining terminal Cl(1) atoms form bent bridges (~132°) in interlinking the two types of cluster chains and creating the relatively open framework shown in Figure 1. These bridges appear equally strong so that the network could also be described, with some loss of simplicity, in terms of chains of mixed cluster types connected by Cl(1).

The Zr–Cl^i distances in both clusters are typical and about the sum of the six-coordinate crystal radii[15] for Zr^{4+} and Cl^-, 2.53 Å. The Zr–Cl^{a-a} distances are somewhat longer, as is usual, 2.70 Å in the zigzag chain, 2.60 Å in the linear chain, and an intermediate 2.64 Å for those interconnecting the two chains.

The potassium atom is situated in a ten-coordinate position of mirror symmetry (type a) that is centered between a pair of bridging Cl^{a-a} atoms from the linear and zigzag chains and also contains eight Cl^i atoms from four clusters, two in each chain. As shown in Figure 2, the coordination sphere around the potassium is a distorted bicapped cube, the capping Cl^{a-a} atoms lying over opposite faces. The K–Cl distances tabulated in Table V average 3.42 Å, nearly equal to the sum of the appropriate crystal radii, 3.40 Å.

In addition to the site occupied by the potassium atom, two other potential cation sites exist within the interlinked cluster framework. These each have half the multiplicity and are used exclusively when a larger cation is present. Such is the case in the parent structure $CsNb_6Cl_{15}$, where these two sites are fully occupied and the smaller potassium site is completely empty.[14] It is evident from a comparison of calculated and observed Guinier powder diffraction patterns that both $RbZr_6Cl_{15}C$ and $CsZr_6Cl_{15}C$ also adopt this alternate placement of cations (supplementary material). The observed *decrease* in the unit cell volume between $KZr_6Cl_{15}C$ and these two heavier analogues (Table I) is also consistent with the occupation of the larger, alternative set of cation sites. The nature of the larger cation sites will be examined in detail in connection with the structure of $CsKZr_6Cl_{15}B$.

$CsKZr_6Cl_{15}B$. This phase has been studied by single-crystal X-ray diffraction in order to confirm the occupation of and the ordering between the cation sites. Structurally, $CsKZr_6Cl_{15}B$ exhibits the same orthorhombic symmetry and metal–halogen skeleton as do $KZr_6Cl_{15}C$ and $CsNb_6Cl_{15}$ (Figure 1). The difference lies, as expected, in the identity of the interstitial atom with the resulting changes in distances and in the simultaneous occupation of all three cation sites. The Zr–Zr and Zr–Cl^i distances are all slightly longer than in the carbide, a result of the cluster expansion necessary to accommodate the larger boron interstitial. The Zr–B distances average ~2.31 Å, giving as before an effective crystal radius of 1.45 Å for boron, slightly larger than that seen for carbon. Relatively few simple borides exist without B–B bonding, making a meaningful comparison of the observed Zr–B distance with other structures difficult. A small sample of NaCl-type zirconium and hafnium borides, mixed boride nitrides and boride carbides[17] yields an effective boron radius of 1.46 Å, which compares nicely with the observed boron radius in these and other zirconium chloride cluster phases like $Zr_6Cl_{14}B$, $K_2Zr_6Cl_{15}B$,[1] and $Rb_5Zr_6Cl_{18}B$.[10]

The crystallographic results for $CsKZr_6Cl_{15}B$ clearly show that all three cation sites in the structure are occupied. The refined nominal occupancies, 1.27 (1), 0.937 (6), and 0.784 (6), for neutral atoms in the smaller potassium site (a) and the two larger cesium sites (b), respectively, are indicative of a small amount of cation mixing, primarily between the K and Cs(2) positions. Consideration of the atomic numbers, multiplicities, and refined occupancies indicates that, as a whole, the present structure contains 71.5 e/formula unit for the cations compared with the expected value of 74 e for the indicated composition. These occupancies allow estimates of the cation distribution among sites, namely, ~14% cesium on the potassium site with ~10% potassium on the cesium(1) site and ~33% on the cesium(2) site.

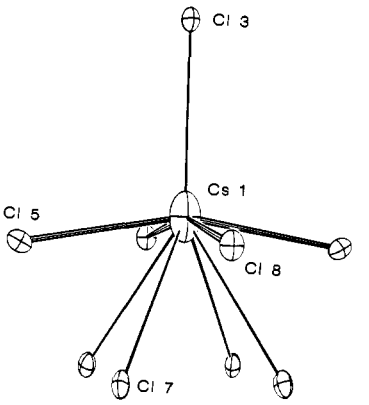

Figure 3. The cesium(1) site in $CsKZr_6Cl_{15}B$. The *c* axis is vertical, the Cl(5) and Cl(8) atoms lie on perpendicular mirror planes, and Cl(3) at the top bridges the zigzag chain (50% ellipsoids).

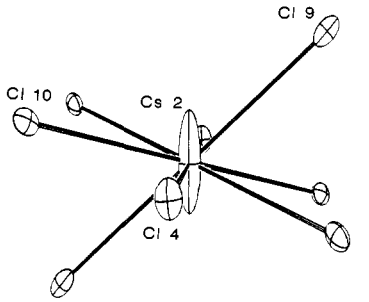

Figure 4. The cesium(2) site in $CsKZr_6Cl_{15}B$ as refined in space group *Pmma*. A mirror plane through Cs(2) and Cl(9) lies approximately in the plane of the paper with a twofold axis through Cl(4) and Cs(2) (50% ellipsoids).

Dimensionally, the smaller site occupied by potassium in the boride is nearly identical with the corresponding position in $KZr_6Cl_{15}C$, the 0.02-Å increase in the average K–Cl distance probably reflecting the expansion of the anion matrix because of the larger boron interstitial.

Cesium Sites. The pair of contrasting type (b) cation positions are quite interesting because of the very unusual coordination environment each provides for the larger cesium. Their locations are marked in Figure 1 by small solid and open circles for Cs(1) and Cs(2), respectively. The Cs(1) site is approximately square pyramidal in shape, as shown in more detail in Figure 3. It lies on the intersection of two mirror planes at $^1/_4$, $^1/_4$, *z* and is approximately centered between Cl(8) atoms on clusters in adjacent linear chains. The atom sits ~0.5 Å above the least-squares plane of Cl(5) and Cl(8) atoms that form the base of a square pyramid (planar within ±0.05 Å) with Zr–Cl distances of 3.463 (3) and 3.531 (3) Å. The sum of six-coordinate radii is 3.48 Å. The fifth atom at the apex of the pyramid, Cl(3), lies directly over the cesium at a distant 3.935 (5) Å, leaving the cation essentially four-coordinate. Four additional Cl(7) atoms lie in a plane below the pyramid base at comparable distances of 3.960 (3) Å from the cesium. The B_{33} value for cesium along the pseudo-fourfold axis of the pyramid is about 3 times the average perpendicular value, a plausible result.

In $CsNb_6Cl_{15}$, the cesium atom sits nearly 0.5 Å higher above the pyramidal base, correspondingly shortening the distance to the apex chlorine and giving five more nearly equal distances.[14] This striking difference between the two compounds appears to be largely a consequence of the change in the interlinked cluster matrix, the dimensions of the average $Zr_6Cl_{12}B$ cluster being 10–15% greater than those of the niobium analogue. The increased cluster size creates increased nonbonded Cl–Cl distances and larger voids, particularly between chlorine atoms on different clusters such as the basal Cl(5) and Cl(8) atoms in the pyramid. This requires that the cesium in the zirconium phase move closer to the pyramid base in order to retain four comparable Cs–Cl dis-

(17) Pearson, W. B. *The Crystal Chemistry and Physics of Metals and Alloys*; Wiley-Interscience: New York, 1972.

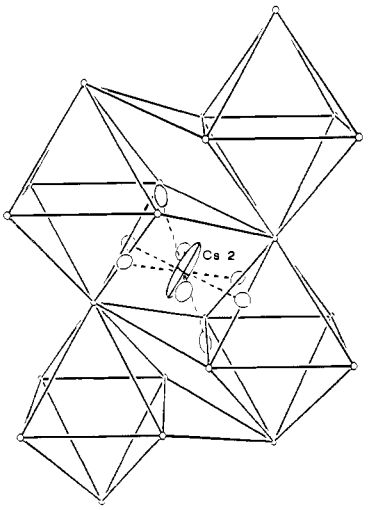

Figure 5. A larger, approximately [0$\bar{1}$0] view of the cesium(2) site between polyhedra defined by chlorine atoms on neighboring clusters. Small circles are cluster-bridging Cl^a; larger ellipsoids are the nearest-neighbor Cl^i atoms in Figure 4. The solid lines define chlorine polyhedra and their contacts, not bonds.

tances but at the expense of the one Coulombic interaction with the apex chlorine.

The second cesium atom is even more unusual in its coordination geometry. As shown in Figure 4, it resides in or near an eight-coordinate position of $2/m$ symmetry along $\vec{a}$ and midway between linear cluster chains. Four Cl(9) and two Cl(10) atoms from clusters within those chains form a very elongated trigonal antiprism with Cs–Cl distances of 3.514 (2) Å [×4] and 3.566 (3) Å [×2]. The two remaining Cl(4) atoms that also bridge cluster edges within the zigzag chain lie on a twofold axis normal to the long axis of the antiprism and give the shortest Cs–Cl distances, 3.440 (2) Å. There are no other neighbors within 4.8 Å. The Cs(2) atom in such an asymmetric environment refines with the extremely elongated ellipsoid shown that protrudes out opposites faces of the trigonal antiprism perpendicular to its (pseudo) $\bar{3}$ axis. An alternate description, which better illustrates the unusual coordination about the cesium atom, starts with the note that the cesium atom lies in a rigorous plane of six chlorine atoms. The remaining Cl(9) atoms lie on a line through the cesium atom that intersects the plane of the six chlorine atoms at an angle of ~55°. The cesium ellipsoid is essentially elongated perpendicular to the plane but slightly canted away from the Cl(9) atoms lying above and below it.

A larger view of the surroundings about the cesium(2) site is shown in Figure 5 in terms of just the chlorine atoms in neighboring clusters. The figure emphasizes that the structural framework defining the Cs(2) cavity leaves it tightly girded around the waist but relatively open in the [101] direction. Some twisting (torsion) of the host matrix can also be imagined, particularly if the problem cation were to order, and a harmonic description of the cation distribution may not be suitable. The apparent disorder of a cation at this site is thus a logical consequence of the structure, a problem that should extend to other compounds that utilize this site, i.e., $RbZr_6Cl_{15}C$, $CsZr_6Cl_{15}C$, $Rb_2Zr_6Cl_{15}B$, and $CsRbZr_6Cl_{15}B$. The same disorder occurs in $CsZr_6Cl_{15}Fe$,[18] where there are even larger clusters, and should also in $CsZr_6Br_{15}Fe$[10] unless the present potassium site becomes sufficiently large to accommodate cesium.

The most simplistic view of the refinement results for the two cesium sites, particularly the second, is that a number of positions are occupied in the asymmetric array produced by a somewhat flexible anion matrix. The collection of problem thermal ellipsoids found at first suggested that the structure had been refined with too high an imposed symmetry, but no solution could be found in any of the lower symmetry space groups that were consistent with the general character of the structures (see Experimental Section and supplementary material). A plausible but presently unprovable explanation of these difficulties is that all of the crystals available are twinned via alternative displacements of cations, Cs(2) in particular, and this is accompanied by small shifts of the neighboring chlorine environment and possibly some small twisting of the cluster matrix as well. Some probable potassium occupancy of the Cs(2) site is an additional complication. We are fortunate to have the $KZr_6Cl_{15}C$ example so as to better define the structural arrangement.

(18) Zhang, J.; Corbett, J. D., unpublished research.

Table VI. Distribution of Bridging Halide Angles in $M_6X_{12}X_{6/2}$-Type Structures

structure type	space group	other examples	$Cl^{a\text{-}a}$ bridge type, % linear	bent	ref
Ta_6Cl_{15}	*Ia3d*	$Zr_6Cl_{15}N$, $Na_2Zr_6Cl_{15}B$[a]	0	100	1, 10, 15
$CsNb_6Cl_{15}$[b]	*Pmma*	$KZr_6Cl_{15}C$,[c] $CsKZr_6Cl_{15}B$,[b,c] $(Cs,Rb)Zr_6Cl_{15}C$[b]	17	83	this work, 1, 14
$K_2Zr_6Cl_{15}B$	*Cccm*	$K_2Zr_6Cl_{15}Be$	33	67	1, 10
$K_3Zr_6Cl_{15}Be$	*C2/c*	$Rb_3Zr_6Cl_{15}Be$	33	67	10
Nb_6F_{15}	*Im3m*	$Zr_6Cl_{15}Co$	100	0	18, 19

[a] Slight tetragonal distortion. [b] Large cation sites (b). [c] Small cation site (a).

Discussion

The structure described here represents first a new arrangement for some old examples, namely, M_6X_{12} clusters interconnected at all vertex positions by bridging halides to give an $(M_6X_{12})X_{6/2}$ stoichiometry. The present arrangement is evidently generated so that alkali-metal cations can also be accommodated, but the sites available within this cluster anion framework do not always provide ideal environments for that purpose, as first shown for $CsNb_6Cl_{15}$.[14] This particular structure is also unusual because it furnishes the first description of linearly bridged clusters $-(Zr_6Cl_{12}Z)-Cl-$ in any halide system other than in Nb_6F_{15}. Equally important, the necessity of an interstitial atom within the cluster introduces a new variability to the chemistry possible.

The presence of two sets of cation sites that are separately and completely occupied in $KZr_6Cl_{15}C$ and $CsNb_6Cl_{15}$ depending on the cation size first provided the impetus to prepare compounds containing two different cations, one on each set. The addition of another cation within the framework might be achieved either by a one-electron reduction of each cluster or by a compensating increase in non-metal charge. The addition of another electron to the cluster bonding orbitals seemed unlikely on the basis of our experience with numerous zirconium chloride clusters as these show a marked proclivity for 14 cluster-bonding electrons.[1] Attempts to add additional electrons often produced a compensating increase in the Cl:Zr ratio in the phase even under mildly reducing conditions, although a few 15-electron clusters have been recently obtained, the present $KZr_6Cl_{15}N$ among them. Although an increase in nonmetal charge without change in electron count could potentially be accomplished by substitution of chalcogenide for chloride, the replacement of the interstitial carbon atom with boron is operationally much more facile. Indeed, reactions with halides of the cation pairs CsRb, CsK, and Rb_2 all proceed readily in the presence of boron and give essentially quantitative yields of $MM'Zr_6Cl_{15}B$ in the desired structure.

M_6X_{15} Structure Types. The phases $KZr_6Cl_{15}C$ and $CsKZr_6Cl_{15}B$ show a structural behavior that is typical for M_6X_{15} compounds. Differences among the five M_6X_{15} structure types now known are not in the style of the local connectivity, which is always $M_6X^i_{12}X^{a\text{-}a}{}_{6/2}$, but rather in the larger three-dimensional connectivity of these, the local $X^{a\text{-}a}$ geometry and, of course, the lattice symmetry. These are summarized in Table VI.

The general structure type found for $KZr_6Cl_{15}C$ and $CsKZr_6Cl_{15}B$ occupies an intermediate position in the M_6X_{15} series in an important three-dimensional variable, the local geometry at the six $X^{a\text{-}a}$ bridges. The Ta_6Cl_{15} structure,[15] which includes

the relevant $Zr_6Cl_{15}N$ and $Na_2Zr_6Cl_{15}B$ examples,[1,10] occurs at one end of the series and has only bent X^{a-a} bridges joining the clusters, while Nb_6F_{15}[19] at the opposite end contains only linear X^{a-a} bridges. Other M_6X_{15}-type compounds exhibit varying combinations of bent and linear X^{a-a} bridges; $CsNb_6Cl_{15}$, $KZr_6Cl_{15}C$, $CsKZr_6Cl_{15}B$, and the like (Table I) have one-sixth linear X^{a-a} bridges, the remainder bent, and two other $M_6X_{12}X_{6/2}$-type structures, $K_2Zr_6Cl_{15}B$ and $K_3Zr_6Cl_{15}Be$, both show one-third linear bridges.[1,10]

One of the key factors that differentiate among the various M_6X_{15}-type structures is the size and number of cation that must be accommodated in the structure. The introduction of linear X^{a-a} bridges tends to create larger voids within the structure and consequently room for more and larger cations, or vice versa. The trend is nicely illustrated going from Ta_6Cl_{15}, with no linear bridges, to $CsKZr_6Cl_{15}B$, with one-sixth linear bridges, to Nb_6F_{15}, with all linear bridges. The Ta_6Cl_{15} structure presently appears to be limited either to compounds containing no cations, such as Ta_6Cl_{15} and $Zr_6Cl_{15}N$,[1] or to those compounds that contain small cations, $Na_{0.5}Zr_6Cl_{15}C$[1] and $Na_xNb_6Cl_{15}$, $x < 1$,[14] being examples. In contrast, the $CsNb_6Cl_{15}$ structure has been obtained only in compounds containing one cation as large as potassium or, if with two cations, with at least one as large as rubidium. Exploration of many of the possibilities in this case are described in this paper. Finally, in Nb_6F_{15} the voids have become so large that it is possible/necessary to fill these with a second interpenetrating lattice of Nb_6F_{15} clusters.

Although exhibiting the same local connectivity around each cluster, the three M_6X_{15} structure types Ta_6Cl_{15}, $CsNb_6Cl_{15}$ (as represented by $KZr_6Cl_{15}C$), and Nb_6F_{15} are not related in a larger three-dimensional sense. In other words, the three structures cannot be interconverted simply by rotation of clusters and bending of bonds at bridging chlorines, i.e., without breaking $M-X^{a-a}$ bonds. Their inequivalence can be seen by starting at a Cl^{a-a} atom in the zigzag chain in $KZr_6Cl_{15}C$ and following the shortest bonding path through the structure back to the starting point, without retracing. In this case the shortest path is by way of three clusters in the sequence $(Zr-Zr-Cl^{a-a})_3$ (Figure 1). In the Ta_6Cl_{15} type, the shortest sequence that can be found starting at any Cl^{a-a} (since they are all equivalent by symmetry) is $(Ta-Ta-Cl^{a-a})_4$. The Nb_6F_{15} structure is inequivalent to both structures, being composed instead of two interpenetrating lattices. The other two structure types in Table VI, $K_2Zr_6Cl_{15}B$ and $K_3Zr_6Cl_{15}Be$, are related to one another but not to the remainder. These will be described subsequently.[10]

Bonding. The bonding in these and other interstitially stabilized clusters, both isolated and condensed, is largely dominated by strong, covalent metal-to-interstitial bonds. From a molecular orbital standpoint,[1-4,10] the 2s and 2p orbitals for carbon, boron, etc. interact strongly with the metal–metal bonding orbitals of a_{1g} and t_{1u} symmetry available in the empty octahedral cluster to form four corresponding, low-lying metal–interstitial bonding orbitals plus their high-lying antibonding counterparts. The remaining t_{2g} and the higher lying a_{2u} metal–metal bonding orbitals of the empty cluster carry over unchanged to the filled cluster to provide a total of eight metal–metal and metal–interstitial cluster bonding orbitals, the same number as in the empty cluster. Four additional valence electrons from the interstitial carbon have thus been added to the cluster bonding manifold. But a charge transfer from the interstitial atom to the metal framework is by no means implied and is undoubtedly far from the truth. Extended Hückel calculations for both isolated clusters and a condensed sheet of clusters[1,2,10,20] as well as XPS core data for carbon 1s[11] indicate that the interstitial carbon atom is somewhat negatively charged. In the case of $Zr_6Cl_{14}C$, the carbon binding energy shift is −3.0 eV.[10]

For the purpose of counting electrons, the cluster electron count is equal to the sum of the metal, cation, and interstitial valence electrons minus the number of chlorine atoms since the chlorine valence orbitals are filled. (PES data show that they lie ~6 eV below the HOMO or E_F.[20]) For $KZr_6Cl_{15}C$ the cluster electron count is therefore $1 + 6\,(4) - 15\,(1) + 4 = 14$. In the vast majority of cluster compounds containing interstitial elements, only the first seven of eight cluster bonding orbitals are filled, presumably because of the $M-X^i$ antibonding contributions in the eighth a_{2u} orbital, although a small number of 15- and 16-electron clusters are known.[1,2,10]

The rare-earth and early transition metals appear to be uniquely suited for the preparation of interstitially stabilized clusters owing to both their relative lack of valence electrons and the large radial extension of the metal's valence orbitals. The apparent incompatibility of M_6X_8-type clusters with centered atoms (except for hydrogen[21,22]), probably because of potentially small interstitial–X^i separations, limits interstitially stabilized clusters primarily to those of an M_6X_{12}-type and hence to a maximum of 16 cluster electrons. For the metal halides, this effectively limits the cluster metal to one containing four or fewer valence electrons, essentially those from groups III and IV plus the lanthanide and actinide elements. The use of higher charged anions such as the chalcogenides would allow expansion of the potential cluster metals to groups V and VI, but the metal–metal overlap in clusters of a size necessary to accommodate most interstitial atoms would fall off significantly. Whether the phases are indeed unstable has not been well-explored. Working within these constraints, however, a considerable amount of exciting chemistry has been and remains to be discovered.

Acknowledgment. We are indebted to Dr. Imoto and Professor Simon for their kind communication of the $CsNb_6Cl_{15}$ results prior to publication and to Professor R. A. Jacobson for the continued provision of diffraction and computing facilities. This research was supported by the National Science Foundation, Solid-State Chemistry, via Grant DMR-8318616 and was carried out in facilities of the Ames Laboratory, DOE. R.P.Z. was also the holder of Departmental Proctor and Gamble and Gilman Fellowships.

Supplementary Material Available: Tables of anisotropic thermal parameters for $KZr_6Cl_{15}C$ and $CsKZr_6Cl_{15}B$, details of alternate space groups and refinements considered for $CsKZr_6Cl_{15}B$, and the observed and calculated Guinier powder patterns for $CsZr_6Cl_{15}C$ (6 pages); listings of observed and calculated structure factor data for $KZr_6Cl_{15}C$ and $CsKZr_6Cl_{15}B$ (12 pages). Ordering information is given on any current masthead page.

(19) Schäfer, H.; Schnering, H.-G.; Niehues, K.-J.; Nieder-Vahrenholz, H. G. *J. Less*-common *Met.* **1965**, *9*, 95.

(20) Ziebarth, R. P.; Hwu, S.-J.; Corbett, J. D. *J. Am. Chem. Soc.* **1986**, *108*, 2594.

(21) Imoto, H.; Corbett, J. D. *Inorg. Chem.* **1980**, *19*, 1421.

(22) Imoto, H.; Simon, A. *Inorg. Chem.* **1982**, *21*, 308.